Journal of Alloys and Compounds 686 (2016) 347–355

Contents lists available at ScienceDirect

Journal of Alloys and Compounds

journal homepage: http://www.elsevier.com/locate/jalcom

Effect of Al addition on microstructure, texture and mechanical properties of Mg-5Gd-2.5Y-2Zn alloy

Canfeng Fang*, Guangxu Liu, Hai Hao, Zhiheng Wen, Xingguo Zhang

Key Laboratory of Solidification Control and Digital Preparation Technology (Liaoning Province), School of Materials Science and Engineering, Dalian University of Technology, Dalian 116024, China

ARTICLE INFO

Article history:
Received 20 April 2016
Received in revised form
31 May 2016
Accepted 6 June 2016
Available online 7 June 2016

Keywords:
Mg-5Gd-2.5Y-2Zn alloy
Al
Microstructure
Texture
Mechanical properties

ABSTRACT

In this paper, microstructure, texture and mechanical properties of as-rolled Mg-5Gd-2.5Y-2Zn-*x*Al (x = 0, 0.5, 1.0 and 1.5 wt%) alloys were investigated. It was found that the added Al changed the solidification and precipitation behaviour of the matrix alloy by the formation of the Al-RE ($Al_{11}(Y, Gd)_3$ and $Al_2(Y, Gd)$) phases. Edge and surface cracks happened in the as-rolled Mg-5Gd-2.5Y-2Zn alloy disappeared after adding Al. Both the broken W phase and the two Al-RE particles can stimulate nucleation of dynamic recrystallization via particle stimulated nucleation (PSN) mechanism. The content, size and distribution of second phase particles were affinitive with the effect of PSN mechanism, and then affected the texture characteristics, such as intensity and orientation distribution. The elongation of the Mg-5Gd-2.5Y-2Zn alloy was pretty low, just about 4.4%. After the addition of Al, although there was a slight decrease in strength, the ductility was obviously increased. Especially, the elongation of the alloy with 1.0 wt% Al addition was about 16.4% which approached 4 times as high as the Mg-5Gd-2.5Y-2Zn alloy. Besides, Al addition significantly changed the fracture surface of the Mg-5Gd-2.5Y-2Zn alloy. In particular, as 1.0 wt% and 1.5 wt% Al was added, many deep dimples were clearly observed, which showed obvious ductile characteristics.

1. Introduction

Mg-Zn-RE (RE, rare earth) system alloys have attracted significant interests because of their excellent mechanical properties at both room and elevated temperature [1–4]. It is generally known that there are three kinds of ternary equilibrium phases in Mg-Zn-RE system alloys, i.e. W phase ($Mg_3Zn_3RE_2$, cubic structure), I phase (Mg_3Zn_6RE, icosahedral quasicrystal structure) and X phase ($Mg_{12}ZnRE$, long-period stacking order (LPSO) structures) [2,3]. Among them, I phase and X phase were believed to be effective reinforcement phases and obtained much more attention [4,5]. However, due to the weak bonding with Mg matrix [4] and the tendency to crack during the tensile process [6], the W phase is generally considered as a destructive phase rather than an instructive one. So, it is necessary to control the volume fraction of W phase by optimizing Zn/Y (wt%) ratio [4] and/or carry out reasonable thermomechanical working process [7] to obtain ideal mechanical properties of Mg-Zn-RE alloys.

Al_2Y intermetallic compound can be in-situ formed by the reaction between Al and Y elements in molten Mg alloys. Recently, lots of attention has been paid to the refining ability of the in-situ Al_2Y, and subsequent improvement in mechanical properties [8–10]. Qiu et al. [8] reported that an addition of 0.6–1.0 wt% Al into the Mg-10 wt% Y melt promoted the in-situ formation of Al_2Y, which reduced the average grain size from 180 to 36 μm. And the active nucleation Al_2Y particles were reproducibly observed at the centres of many refined grains. Moreover, Zhao et al. [9] investigated the influence of Y on AZ91D alloy and their results showed that the addition of Y led to the precipitation of rod-shaped Al_2Y phase and exerted a favorable influence on reducing grain size of the AZ91D alloy in both as-cast and extruded states. Tensile tests confirmed that the dramatic increase of the ultimate tensile strength, yield strength and elongation profited from the matrix grain refinement by Al_2Y phase. Similarly, reports by Sun et al. [10] showed that adding Y to the Mg-5Li-3Al-2Zn alloy also resulted in the formation of Al_2Y compound and caused grain refinement of the matrix. The tensile strength and ductility reached peak values when the Y additions were 0.8 wt% and 1.2 wt%, respectively.

Accordingly, a typical Mg-5Gd-2.5Y-2Zn alloy, containing a large

* Corresponding author.
E-mail address: fcf@dlut.edu.cn (C. Fang).

http://dx.doi.org/10.1016/j.jallcom.2016.06.031
0925-8388/

amount of W phases distributed along the grain boundaries of α-Mg, was chosen as the target alloy in the present study. Then, Al element was added to modify the content, shape and distribution of the W phases by the formations of the Al-RE intermetallic phases. Later, the effect of the as-cast microstructure evolution on the rollability, texture and mechanical properties of the as-rolled alloys was primarily studied.

2. Experimental procedures

Commercially pure Mg, Zn, Al, and Mg-30 wt%Gd and Mg-30 wt %Y master alloys were used to prepare the Mg-5Gd-2.5Y-2Zn-*x*Al ($x = 0, 0.5, 1.0, 1.5$ wt%) alloys. The fusion metallurgy was carried out in a mild steel crucible placed in an electric resistance furnace under an anti-oxidizing flux. After melting, the melt was cast into a steel mold at 730 °C. The as-cast alloys were homogenized at 500 °C for 10 h, cooled down in air condition, and then machined into rectangular shape with dimension of 100 × 80 × 18 mm^3. Before hot-rolling, the as-homogenized samples were preheated at the temperature of 485 °C for 30 min. Cross-rolling where each rolling direction changes at 90° (Fig. 1) was conducted at 485 °C. After each rolling pass, the as-rolled samples were reheated to the rolling temperature. Finally, a total plastic deformation of 70% was reached, and then the as-rolled sheets were subjected to air cooling.

The chemical compositions of alloys were analyzed by an X-ray fluorescence analyzer (XRF, XRF-1800), and the results are listed in Table 1. The phase analysis and macro-texture tests were performed by an X-ray diffraction (XRD, Empyrean) with Cu Kα radiation. Energy dispersive X-ray spectroscopy (EDS) was also used to determine the phases formed in the samples. The microstructures were observed by an optical microscope (OM, Leica MEF4) and a scanning electron microscope (SEM, SUPRA 55). The specimens for the OM and SEM observation were prepared following a standard procedure of grinding, polishing and etching (1.0 g picric acid + 2 ml acetic acid + 3 ml water + 20 ml ethanol). The average grain size was evaluated by using the mean linear intercept method [11,12].

Tensile test was carried out by using a DNS100 universal testing machine with a strain rate of $1 \times 10^{-3} s^{-1}$ at room temperature. Each material used for repeat tensile tests was cut into three samples with their long axes parallel to the RD1. The fracture surfaces were also observed by the SUPRA 55 SEM.

3. Results and discussions

3.1. Microstructures of the as-cast alloys

Fig. 2 shows the XRD patterns of the as-cast Mg-Gd-Y-Zn-*x*Al series alloys. It is revealed that the Alloy I consisted of α-Mg and W phase ($Mg_3Zn_3(Y, Gd)_2$), while the alloy with minor Al (about 0.5 wt %) addition consisted of three phases: α-Mg, W phase and $Al_{11}(Y, Gd)_3$ phase. With increasing Al content to 1.0 wt%, the diffraction peaks of $Al_{11}(Y, Gd)_3$ phase were intensified obviously, whereas the amount of W phase decreased comparatively. When the amount of Al was 1.5 wt%, diffraction peaks of $Al_2(Y, Gd)$ phase were observed distinctly.

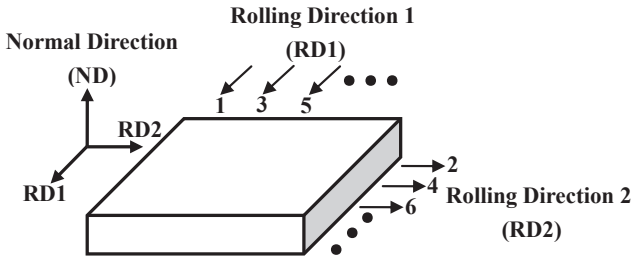

Fig. 1. The schematic diagram of the cross-rolling.

Table 1
Chemical compositions of the as-cast Mg-5Gd-2.5Y-2Zn-*x*Al ($x = 0, 0.5, 1.0, 1.5$).

Designation	Nominal alloys	Compositions (wt%)				
		Gd	Y	Zn	Al	Mg
Alloy I	Mg-5Gd-2.5Y-2Zn	5.02	2.55	1.98	0	Bal.
Alloy II	Mg-5Gd-2.5Y-2Zn-0.5Al	5.09	2.46	2.27	0.49	Bal.
Alloy III	Mg-5Gd-2.5Y-2Zn-1.0Al	5.09	2.63	2.12	0.98	Bal.
Alloy IV	Mg-5Gd-2.5Y-2Zn-1.5Al	4.97	2.45	2.19	1.59	Bal.

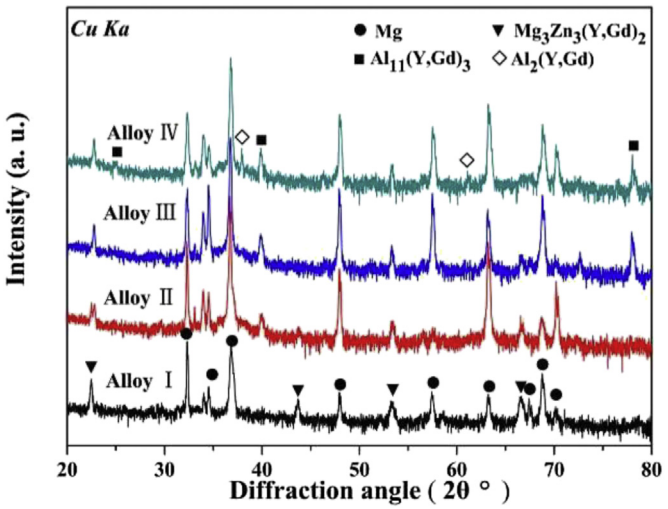

Fig. 2. XRD patterns of the as-cast Mg-Gd-Y-Zn-*x*Al series alloys.

Fig. 3 shows the OM and SEM images of the as-cast alloys. As can be seen from Fig. 3(a), the microstructure of the Mg-5Gd-2.5Y-2Zn alloy was characterized by coarse α-Mg dendrites with plenty of second phases continuously distributed at grain boundary area. Some of the developed second phases were lamellar eutectic structure, as shown in the local magnification of Fig. 3(b). Combining the results of XRD and EDS (not shown in this paper), these second phases were identified to be W phase. Except for W phase, neither I phase nor X phase was detected in the Alloy I. When 0.5 wt% Al was added, the W phases which continuously distributed at the grain boundaries were separated and their amount was reduced to some extent (Fig. 3(c)). Besides, some as-clustered particles could be found around W phases (Fig. 3(c, d) and inset). It is worth noting that the total amount of second phases in the Alloy II decreased obviously comparing with the Alloy I. With increasing Al content to 1.0 wt%, the amount of W phases decreased further, but the as-clustered particles significantly increased, and some of them grew developed and had a flattened tendency (Fig. 3(e, f)). XRD pattern and EDS analysis reveal that the as-clustered particle was $Al_{11}(Y, Gd)_3$. For the Alloy IV (Fig. 3(g, h)), the size and amount of $Al_{11}(Y, Gd)_3$ increased simultaneously, and some polygon particles with an average size of about 10 μm emerged. These polygon particles were identified to be $Al_2(Y, Gd)$.

Comparing the microstructures of Alloy I with Alloy II–IV, it can be concluded that the solidification and precipitation behaviour of the Mg-5Gd-2.5Y-2Zn alloy can be significantly affected by the addition of Al. Specifically, the added Al elements had priority to

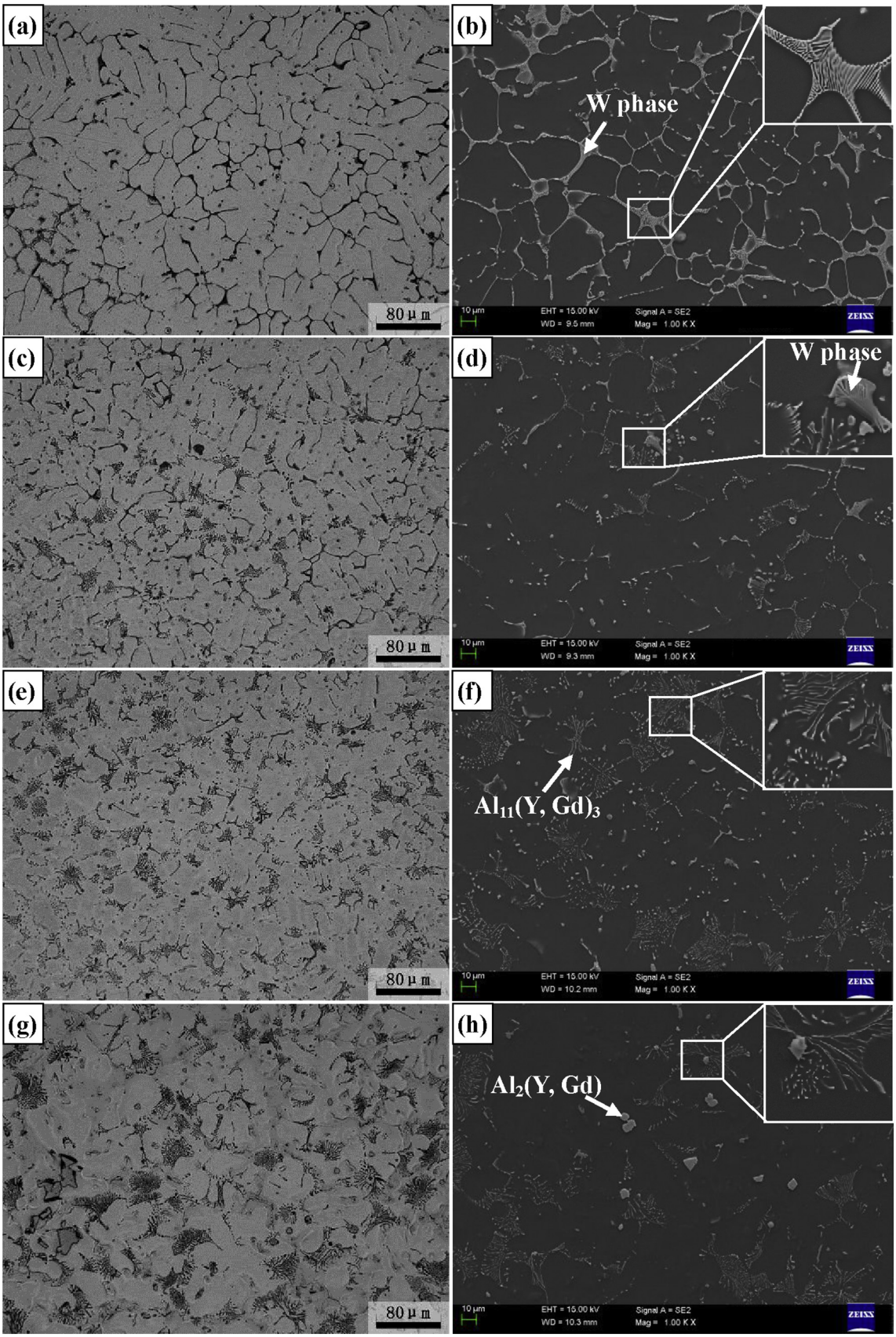

Fig. 3. OM and SEM images of the as-cast: (a) OM image and (b) SEM image obtained from Alloy I; (c) OM image and (d) SEM image obtained from Alloy II; (e) OM image and (f) SEM image obtained from Alloy III; (g) OM image and (h) SEM image obtained from Alloy IV.

react with Gd and Y elements to form $Al_{11}(Y, Gd)_3$ and $Al_2(Y, Gd)$ phases. The generation of the two Al-RE phases led to the increase of Zn/RE (wt%) ratio by reducing the content of Gd and Y elements in alloy system, but this ratio does not reach to the critical value of I phase generation, as the 4.38 mentioned in Ref. [3]. Therefore, the addition of Al just played a role in separating the continuous net-like microstructure and decreasing the amount of W phase, rather than stimulating the appearance of I phase. In addition, with the increase of Al content, the amount of $Al_{11}(Y, Gd)_3$ increased rapidly (Fig. 3(c-h)). $Al_2(Y, Gd)$ particles could be observed when the content of Al element reaches to a certain value (Fig. 3(g, h)).

3.2. Macro-morphology of the as-rolled alloys

Rollability of the Alloy II–IV were all improved due to the addition of Al comparing with the Alloy I. Fig. 4 exhibits the macro-morphologies of RD2-ND and RD1-RD2 planes of the as-rolled Alloy I and Alloy III sheets. Some cracks which rotated 45° from RD2 towards normal direction (ND) of the sheet generated at the edge of the Alloy I (Fig. 4(a, b)). These edge cracks with the average length of about 15 mm expanded toward the inside of the sheet. In addition, there were also some small surface cracks on the RD1-RD2 plane of Alloy I. However, almost all the mentioned cracks could not be found in the Alloy III (Fig. 4(c, d)), indicating a pretty ideal rollability of the Alloy III. Because of the identical rolling process parameters (such as rolling temperature, reduction per pass, etc.) of the Alloy I and the Alloy III, the microstructure changes caused by Al addition, as discussed in Section 3.1, were the key point of the improvement of rollability. The atomic bonding between W phase and Mg matrix was very weak [4], which provided initiation sites for micro-cracking in rolling process. However, after 1.0 wt% Al was added, the content of W phase was obviously decreased followed by the reduction of the weak bonding sites, which correspondingly improved the rollability of Alloy III.

3.3. Microstructures of the as-rolled alloys

The SEM images of RD1-ND plane of the as-rolled alloys are given in Fig. 5. The continuous structure of W phase along grain boundaries disappeared and was replaced by some streamlines consisted of W phase particles with a size of 2 ~ 5 μm (Fig. 5(a)), which indicates that the W phase can be sharply broken by the rolling force. Similar phenomenon was reported by Wang et al. [7]. Fig. 5(b-d) correspondingly shows the SEM images of the as-rolled Alloy II–IV. Comparing with Fig. 3(c-h), it can be found that the as-clustered $Al_{11}(Y, Gd)_3$ particles in the as-cast microstructure were also fragmented and distributed uniformly in the matrix, while there is no difference in the morphology of $Al_2(Y, Gd)$ particles before and after rolling.

Fig. 6 illustrates the OM micrographs of RD1-ND plane of the four alloy sheets. It can be observed from Fig. 6(a) that the grains of the Alloy I sheet were significantly refined (~7 μm) comparing with the as-cast one (Fig. 3(a, b)). The homogeneous and fine equiaxed grains indicate that dynamic recrystallization (DRX) took place during rolling process [13]. This completed DRX microstructure of the Alloy I should be related to the presence of W phase. Because the W phases were broken into fine particles with the size of 2 ~ 5 μm during rolling process (Fig. 5(a)), the enforced strain gradient in the vicinity of non-deformable W phase particles created a region of high dislocation density and large orientation gradient, thus promoting nucleation of recrystallization [14], in which a mechanism called particle-stimulated nucleation (PSN) happened.

Unlike the Alloy I, the as-rolled Alloy II shows a bimodal microstructure consisting of large deformed grain zones and fine DRXed grain zones (Fig. 6(b)). It should be noted that the fine DRXed grain zone was coincided with the particle distribution region. Park et al. [15] concluded that the DRX fraction was influenced by the initial grain size of the as-cast alloys and the PSN mechanism. However, in this study, the grain sizes of the four as-cast alloys are almost the same (Fig. 3), therefore, effect of the initial grain size on DRX fraction can be ignored. As the discussed above, the addition of 0.5 wt% Al resulted in the decrease of particle amount and the inhomogeneous particle distribution (Fig. 3(c, d)), which made the effect of PSN mechanism to be declined and localized. This incompleted DRX caused by the nonuniform particle distribution is similar to the results reported by Shen et al. [12]. As the $Al_{11}(Y, Gd)_3$ particles became enriched and distributed uniformly in the Alloy III matrix (Fig. 3(e, f)), the PSN mechanism happened universally. So, the fraction of DRXed grains in the as-rolled Alloy III further increased but still less than Alloy I (Fig. 6(c)). Moreover, many twins can be found in the as-rolled Alloy III, indicating that

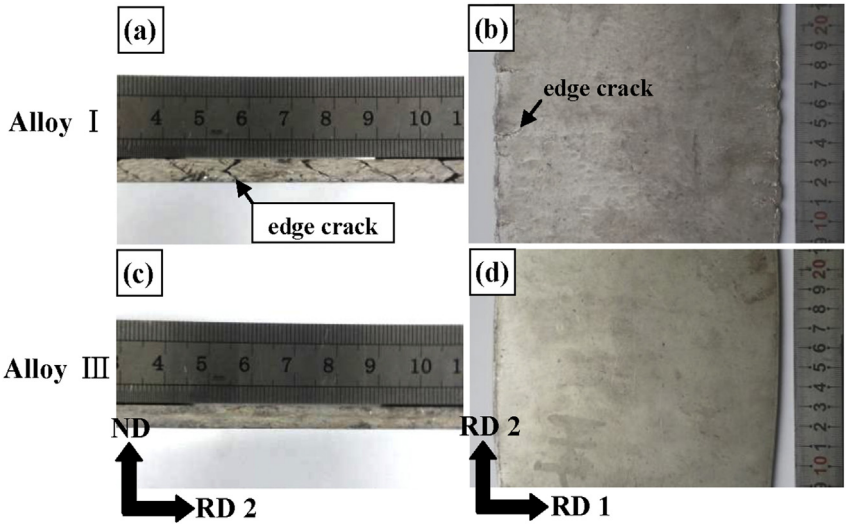

Fig. 4. Macro morphologies of as-rolled sheets obtained from (a) RD2-ND plane of Alloy I, (b) RD1-RD2 plane of Alloy I, (c) RD2-ND plane of Alloy III and (d) RD1-RD2 plane of Alloy III.

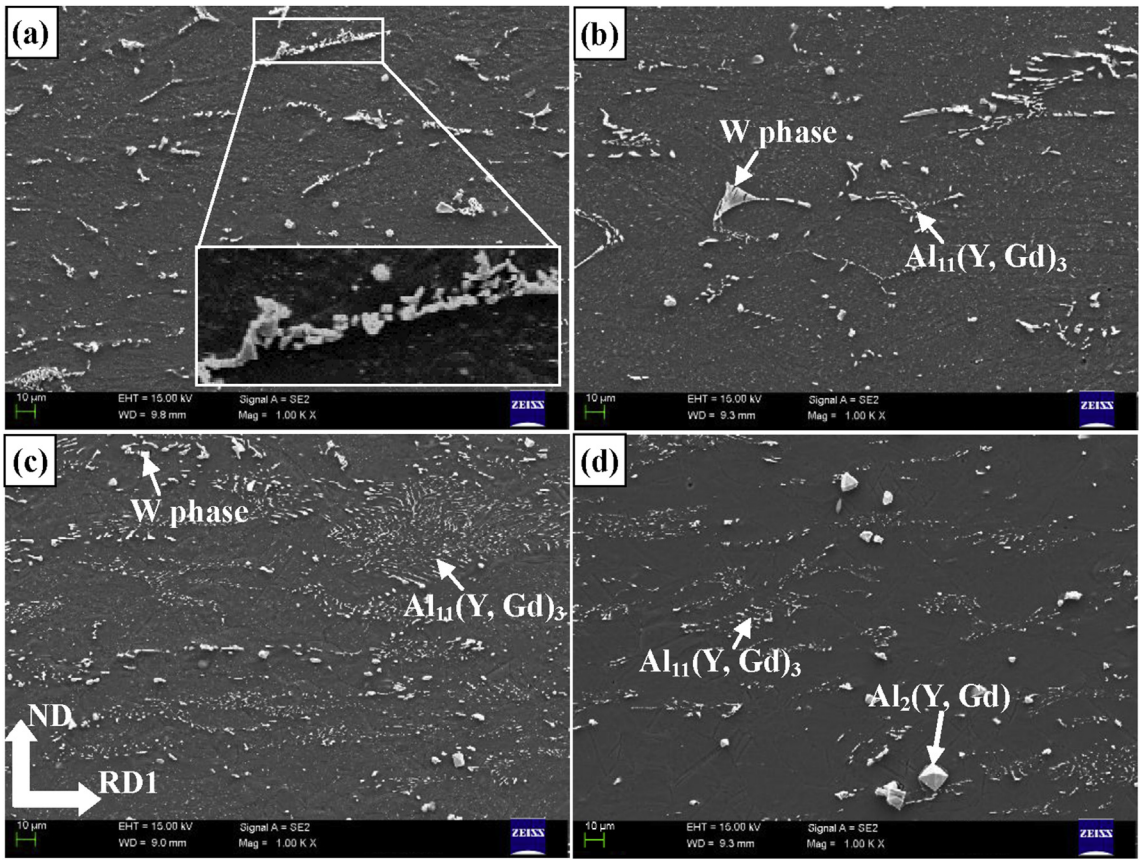

Fig. 5. SEM images of the as-rolled alloy sheets: (a) Alloy I, (b) Alloy II, (c) Alloy III and (d) Alloy IV.

there is difficulty in accommodating the required local high levels of rolling strain by slip alone [16]. It should be emphasized that the microstructure of the as-rolled Alloy IV was made up with pretty coarse equiaxed grains (~25 μm), which was probably ascribed to that the relatively big Al_2(Y, Gd) particles mainly played a role in promoting the growth except for stimulating the nucleation of DRXed grains under our specific rolling conditions, as described in Ref. [17].

3.4. Texture

It had been reported in literature [18,19] that the basal pole in many RE/Y elements containing Mg alloy sheets was easily to spread from normal direction (ND) toward transverse direction (TD), which resulted in the formation a ellipse shape orientation distribution of the (0002) basal texture. However, in the cross-rolling process of this study, because the RD2 and RD1 took turns to serve as the TD in a conventional unidirectional rolling, the basal pole successively spread toward RD2 and RD1. Therefore, the (0002) basal textures of the Alloy I–IV sheets all showed subrotund orientation distribution (Fig. 7(a-d)), which was beneficial to reduce the planar anisotropy between TD and RD [20]. Notably, the orientation distribution of basal poles in the Alloy III was the widest, while it was the narrowest in the Alloy IV and roughly the same in the other two alloys. Furthermore, the Alloy I–III sheets showed a split of the texture peaks from ND toward RD1 and RD2 at the same time, which resulted in the formation of a multi-peak texture (Fig. 7(a-c)). And the scattered degree of the peak intensity distribution increased from the Alloy I to the Alloy III. This RD-tilting characteristic may be considered as the result of activation of pyramidal ⟨c + a⟩ slip [21] or effect of $\{10\bar{1}\ 1\}$-$\{10\bar{1}\ 2\}$ double twinning [22]. However, different from the first three alloys, the as-rolled d Alloy IV exhibited a typical basal texture (Fig. 7(d)), in which the (0002) basal plane of the majority of grains was inclined to be parallel to the sheet plane. The texture type displayed by the Alloy IV was commonly observed in a as-rolled AZ31 alloy [23], and most of them were typical DRX texture.

The comparison of the maximum pole intensity taken from (0002) pole figures of the four alloy sheets is shown in Fig. 7(e). The maximum pole intensity of Alloy I–IV was 7.2, 7.5, 5.1 and 14.7, respectively. According to the literature, the intensity of deformation texture of Mg alloys is associated with not only the completion degree of DRX [7,24] but also the subsequent growth of DRXed grains [25–27]. Comparing with the Alloy I, the DRX in the Alloy II occurred incompletely (Fig. 6(b)), and these unDRXed zones made the maximum pole intensity of the Alloy II to increase slightly. As for the as-rolled Alloy III, its maximum pole intensity was remarkably weakened, which indicated that the effect of Al_{11}(Y, Gd)$_3$ particles on promoting the random orientation of DRXed grains was stronger than W phase particles. Besides, the effect of twinning on texture weakening should not be ignored. Although the DRX in the Alloy IV was very completed, the grains became coarser (Fig. 6(d)). Such grain growth may cause the growth selection of grains with the predominant orientation of basal planes in the sheet plane, which can be seen as the prime reason for the extremely strong texture intensity of the Alloy IV. By the above analysis, we can conclude that there was no linear relation between the Al content and the maximum pole intensity of the sheet. Thus, the rollability of the studied sheet mainly depended on the content of W phase rather than the texture.

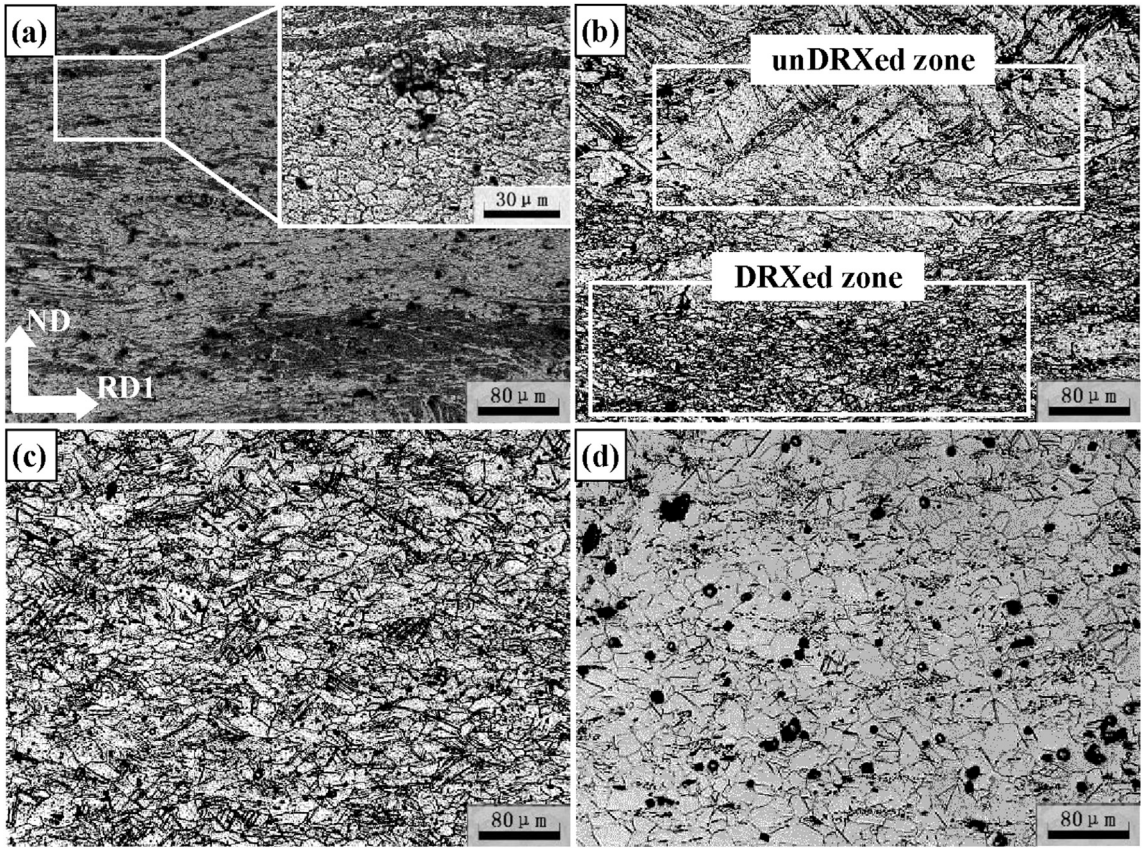

Fig. 6. Optical microscope images of the as-rolled alloy sheets: (a) Alloy I, (b) Alloy II, (c) Alloy III and (d) Alloy IV.

3.5. Mechanical properties

The tensile stress-strain curves of the as-rolled alloys at room temperature are shown in Fig. 8, and the tensile properties, e.g. 0.2% yield strength (YS), ultimate tensile strength (UTS) and elongation (EL) are summarized in Table 2. The YS and UTS of the Alloy I were 258 MPa and 297 MPa, respectively. The addition of 0.5 wt% and 1.0 wt% Al reduced the amount of W phase in grain boundaries of the Alloy II and Alloy III (Fig. 3(c-f) and Fig. 5(b, c)), which would weaken the strength effect of the W phase in the two as-rolled alloys. Besides, the average grain size of both Alloy II and Alloy III increased comparing with Alloy I, lowering the effect of grain refinement strengthening. Therefore, the strength displayed a decreasing tendency from the Alloy I to the Alloy II and the Alloy III. Although the Alloy I showed the highest strength among the Alloy I–III, its EL was pretty low, just about 4.4%. For the reason of this phenomenon, Zhang et al. [4] thought that the weak atomic bonding between W phase and Mg matrix can easily act as initiation sites for micro-cracking in tensile process and deteriorate the ductility. In addition, the strong texture intensity was detrimental to ductility. Fortunately, although the texture intensity of Alloy II increased slightly, the EL of the Alloy II increased about 78% higher than the Alloy I due to the depressed growth of W phase. However, the bimodal as-rolled microstructure limited the strength and ductility of the Alloy II to achieve the optimum. Further improving Al addition, the EL of the Alloy III (16.4%) was improved more obviously and approached 4 times as high as the Alloy I, of which the reason is mainly related to the sharp decrease of W phase, the homogeneous deformation microstructure and the evident texture weakening [7,28]. Interestingly, the strength of the Alloy IV (YS: 225 MPa, UTS: 275 MPa) just slightly decreased compared with the Alloy I, but was higher than the Alloy II and III. Moreover, the EL of the Alloy IV was also much higher than the Alloy I and Alloy II. The unusual tensile properties of the as-rolled Alloy IV may be ascribed to two mixed aspects. One is the homogeneous completed DRX microstructure specially containing tiny W phase, and the other is the unique texture characteristic.

3.6. Fracture behaviour

Fig. 9 shows the SEM fractographs of the as-rolled alloy sheets. The Alloy I exhibited a mixed morphology consisted of cleavage facets and dimples on the fracture surface (Fig. 9(a)). Meanwhile, many aggregated W phase particles are observed. In addition, the depth of dimples containing W phase particles is shallow, indicating that the bond sites between W phase and Mg matrix were weak and easily to become the crack sources in tensile test, which resulted in the comparatively low EL (4.4%). Compared with the Alloy I, the cleavage facet was enlarged and the amount of dimples was decreased (Fig. 9(b)), which can be seen as a result of the presence of the no DRXed zone in the as-rolled Alloy II. However, because of the minor 0.5 wt% Al addition reduced the content of W phase, no obvious aggregated W phase region appeared on fracture surface of the Alloy II. Thus, the EL of the Alloy II was improved in some degree. Because of the homogeneous deformation microstructure of the as-rolled Alloy III and the further lessened destructiveness of W phase, massive deep and fine dimples can be found on the fracture surface of the Alloy III, at the same time, the cleavage facet was rapidly reduced, as shown in Fig. 9(c). This fracture mechanism dominated by ductile fracture sharply enhanced the EL of the Alloy III (16.4%). In addition to $Al_{11}(Y, Gd)_3$ particles, some $Al_2(Y, Gd)$ particles with an average size of 4 μm can

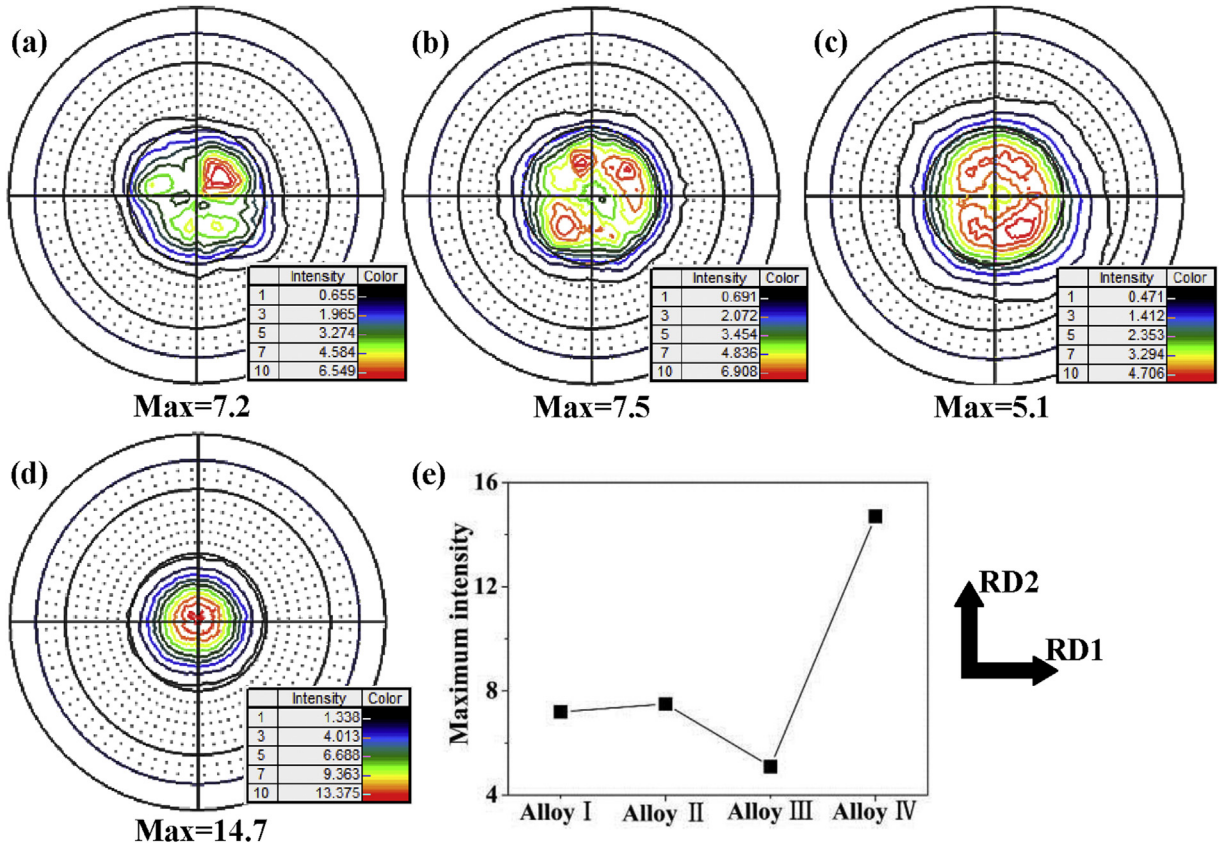

Fig. 7. (0002) pole figures of the as-rolled alloy sheets: (a) Alloy I, (b) Alloy II, (c) Alloy III, (d) Alloy IV and (e) the maximum pole intensity taken from (0002) pole figures.

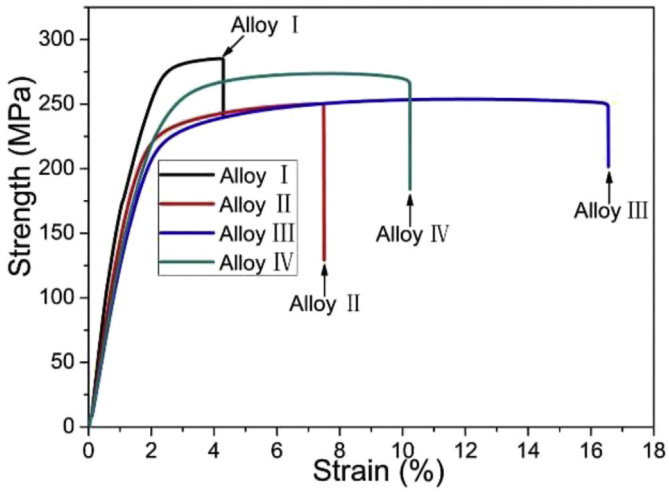

Fig. 8. Stress-strain curves of the as-rolled Alloy I, II, III and IV at room temperature.

Table 2
Tensile properties of the as-rolled Alloy I, II, III and IV at room temperature.

Alloy	UTS (MPa)	YS (MPa)	EL (%)
Alloy I	297 ± 2.1	258 ± 1.9	4.4 ± 0.21
Alloy II	256 ± 4.6	211 ± 2.3	7.5 ± 0.15
Alloy III	257 ± 3.2	208 ± 4.1	16.4 ± 0.11
Alloy IV	275 ± 2.7	225 ± 3.8	10.1 ± 0.24

be found within the dimples of the Alloy III (inset of Fig. 9(c)). It is illustrated that the 1 wt% Al addition could induce the emergence of Al_2(Y, Gd) particles in matrix, which was not obviously displayed in the as-cast microstructure (Fig. 3(e, f)). Similar to the Alloy III, fracture morphology of the Alloy IV is also mainly composed of dimples, which demonstrates a well ductile characteristic as shown in Fig. 9(d). However, the dimple of the Alloy IV was coarser, which may be associated with the coarser DRX grains and the growth of the Al_2(Y, Gd) phases with a quite large size of ~10 μm. These large Al_2(Y, Gd) particles can enhance the local stress concentration, as a result, part of Al_2(Y, Gd) particles were ruptured in tensile process as shown in the inset of Fig. 9(d), which inclined to reduce the EL of the specimen.

4. Conclusion

The effects of Al on microstructure, texture and mechanical properties of Mg-5Gd-2.5Y-2Zn alloy was investigated. Some conclusions can be summarized as follows.

(1) The added Al element had priority to react with Gd and Y elements to form Al_{11}(Y, Gd)$_3$ and Al_2(Y, Gd) phases, which restrained the precipitation and growth of W phase. Accompanied by the decrease of W phase, the amount of Al_{11}(Y, Gd)$_3$ rapidly increased with the increase of Al content. When the content of Al element reached to a certain value, Al_2(Y, Gd) particle was detected clearly by XRD.
(2) Edge and surface cracks easily happened in the as-rolled Mg-5Gd-2.5Y-2Zn alloy. Fortunately, these cracks disappeared after the addition of Al, and the rollability was obviously improved.

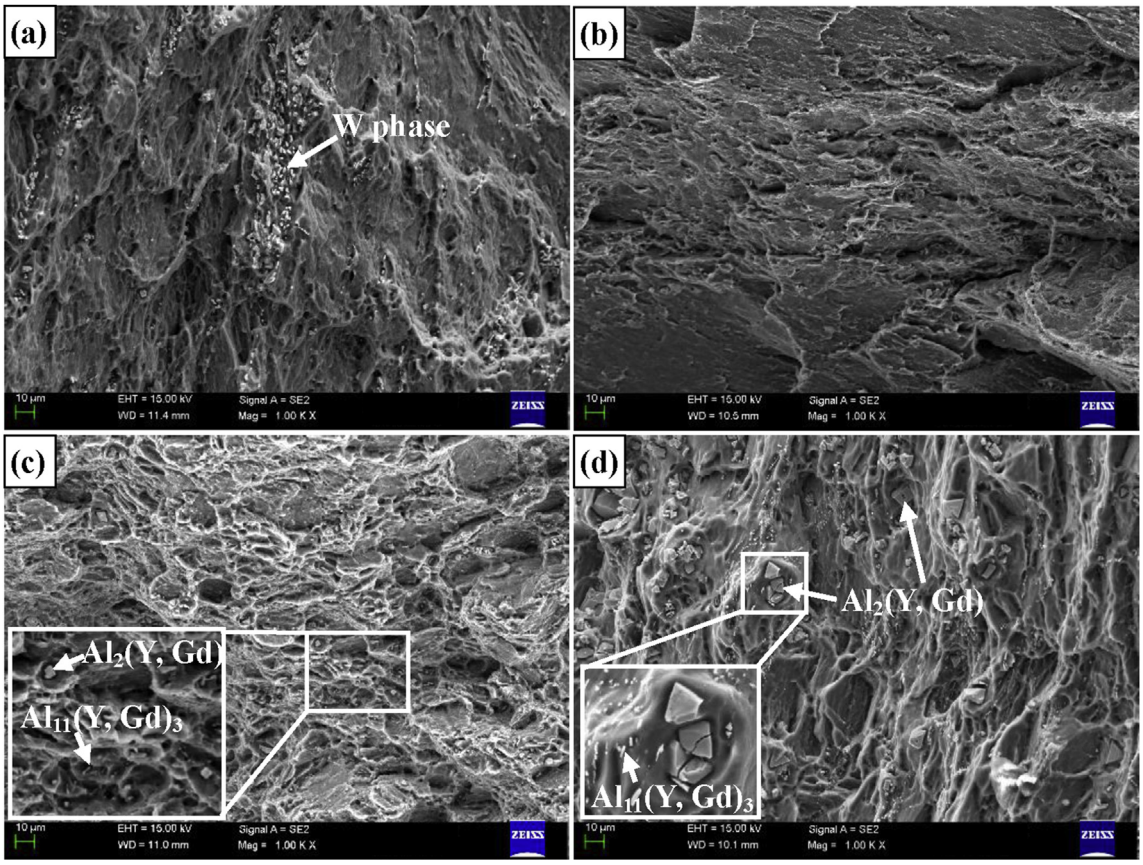

Fig. 9. SEM fractographs of as-rolled alloy sheets (a) Alloy I, (b) Alloy II, (c) Alloy III and (d) Alloy IV.

(3) The continuous net-like W phase and as-clustered $Al_{11}(Y, Gd)_3$ phase in as-cast microstructure were broken into small particles during rolling process, while $Al_2(Y, Gd)$ was insusceptible. All the three kinds of particle phases (W phase, $Al_{11}(Y, Gd)_3$ and $Al_2(Y, Gd)$) can stimulate nucleation of DRXed grains via PSN mechanism.
(4) The content, size and distribution of the second phase particles were affinitive with the effect of PSN mechanism, and then affected the texture characteristics, such as texture intensity and orientation distribution.
(5) The EL of the Alloy I was pretty low, just about 4.4%. After the addition of Al, although there was a slight decrease in strength, the ductility was obviously increased. Especially, the EL of the Alloy III was about 16.4% which approached 4 times as high as the Alloy I.
(6) Al addition significantly changed the fracture surface of the Mg-5Gd-2.5Y-2Zn alloy. In particular, many deep dimples were observed clearly in the Ally III and IV, showing obvious ductile characteristics.

Acknowledgements

The authors gratefully acknowledge the financial support provided by the National Natural Science Foundation of China (No. 51374047), Foundation of Liaoning Educational Committee of China (No. L2013031), and Fundamental Research Funds for the Central University (No. DUT15ZD201 and No. DUT15JJ (G) 01).

References

[1] D. Wu, R.S. Chen, W.N. Tang, E.H. Han, Influence of texture and grain size on the room-temperature ductility and tensile behavior in a Mg-Gd-Zn alloy processed by rolling and forging, Mater. Des. 41 (2012) 306–313.
[2] N. Tahreen, D.F. Zhang, F.S. Pan, X.Q. Jiang, D.Y. Li, D.L. Chen, Hot deformation and processing map of an as-extruded Mg-Zn-Mn-Y alloy containing I and W phases, Mater. Des. 87 (2015) 245–255.
[3] D.K. Xu, L. Liu, Y.B. Xu, E.H. Han, The influence of element Y on the mechanical properties of the as-extruded Mg-Zn-Y-Zr alloys, J. Alloys Compd. 426 (2006) 155–161.
[4] Y. Zhang, X.Q. Zeng, L.F. Liu, C. Lu, H.T. Zhou, Q. Li, Y.P. Zhu, Effects of yttrium on microstructure and mechanical properties of hot-extruded Mg-Zn-Y-Zr alloys, Mater. Sci. Eng. A 373 (2004) 320–327.
[5] M. Yamasaki, T. Anan, S. Yoshimoto, Y. Kawamura, Mechanical properties of warm-extruded Mg-Zn-Gd alloy with coherent 14H long periodic stacking ordered structure precipitate, Scr. Mater 53 (2005) 799–803.
[6] D.K. Xu, W.N. Tang, L. Liu, Y.B. Xu, E.H. Han, Effect of Y concentration on the microstructure and mechanical properties of as-cast Mg-Zn-Y-Zr alloys, J. Alloys Compd. 432 (2007) 129–134.
[7] Q.F. Wang, K. Liu, Z.H. Wang, S.B. Li, W.B. Du, Microstructure, texture and mechanical properties of as-extruded Mg-Zn-Er alloys containing W-phase, J. Alloys Compd. 602 (2014) 32–39.
[8] D. Qiu, M.X. Zhang, J.A. Taylor, P.M. Kelly, A new approach to designing a grain refiner for Mg casting alloys and its use in Mg-Y-based alloys, Acta Mater 57 (2009) 3052–3059.
[9] Z.D. Zhao, Q. Chen, Y.B. Wang, D.Y. Shu, Microstructures and mechanical properties of AZ91D alloys with Y addition, Mater. Sci. Eng. A 515 (2009) 152–161.
[10] C.L. Cui, L.B. Wu, R.Z. Wu, J.H. Zhang, M.L. Zhang, Influence of yttrium on microstructure and mechanical properties of as-cast Mg-5Li-3Al-2Zn alloy, J. Alloys Compd. 509 (2011) 9045–9049.
[11] K.B. Nie, X.J. Wang, K. Wu, X.S. Hu, M.Y. Zheng, Development of SiC_p/AZ91 magnesium matrix nanocomposites using ultrasonic vibration, Mater. Sci. Eng. A 540 (2012) 123–129.
[12] M.J. Shen, X.J. Wang, C.D. Li, M.F. Zhang, X.S. Hu, M.Y. Zheng, K. Wu, Effect of submicron size SiC particles on microstructure and mechanical properties of AZ31B magnesium matrix composites, Mater. Des. 54 (2014) 436–442.
[13] B. Chen, D.L. Lin, X.Q. Zeng, C. Lu, Effects of yttrium and zinc addition on the

microstructure and mechanical properties of Mg-Y-Zn alloys, J. Mater. Sci. 45 (2010) 2510–2517.
[14] R.D. Doherty, D.A. Hughes, F.J. Humphreys, J.J. Jonas, D.J. Jensen, M.E. Kassner, W.E. King, T.R. Mcnelley, H.J. Mcqueen, A.D. Rollett, Current issues in recrystallization: a review, Mater. Sci. Eng. A 238 (1997) 219–274.
[15] S.H. Park, J.G. Jung, Y.M. Kim, B.S. You, A new high-strength extruded Mg-8Al-4Sn-2Zn alloy, Mater. Lett. 139 (2015) 35–38.
[16] J.D. Robson, D.T. Henry, B. Davis, Particle effects on recrystallization in magnesium-manganese alloys: Particle-stimulated nucleation, Acta Mater 57 (2009) 2739–2747.
[17] H. Chang, X.J. Wang, X.S. Hu, Y.Q. Wang, K.B. Nie, K. Wu, Effects of reinforced particles on dynamic recrystallization of Mg base alloys during hot extrusion, Rare Metal. Mater. Eng. 43 (2014) 1821–1825.
[18] J. Hirsch, T. Al-Samman, Superior light metals by texture engineering: optimized aluminum and magnesium alloys for automotive applications, Acta Mater 61 (2013) 818–843.
[19] J. Bohlen, M.R. Nürnberg, J.W. Senn, D. Letzig, S.R. Agnew, The texture and anisotropy of magnesium-zinc-rare earth alloy sheets, Acta Mater 55 (2007) 2101–2112.
[20] Q. Miao, L.X. Hu, G.J. Wang, E.R. Wang, Fabrication of excellent mechanical properties AZ31 magnesium alloy sheets by conventional rolling and subsequent annealing, Mater. Sci. Eng. A 528 (2011) 6694–6701.
[21] S.R. Agnew, M.H. Yoo, C.N. Tomé, Application of texture simulation to understanding mechanical behavior of Mg and solid solution alloys containing Li or Y, Acta Mater 49 (2001) 4277–4289.
[22] B.Q. Shi, R.S. Chen, W. Ke, Effects of yttrium and zinc on the texture, microstructure and tensile properties of hot-rolled magnesium plates, Mater. Sci. Eng. A 560 (2013) 62–70.
[23] A. Styczynski, C. Hartig, J. Bohlen, D. Letzig, Cold rolling textures in AZ31 wrought magnesium alloy, Scr. Mater 50 (2004) 943–947.
[24] L.B. Tong, X. Li, D.P. Zhang, L.R. Cheng, J. Meng, H.J. Zhang, Dynamic recrystallization and texture evolution of Mg-Y-Zn alloy during hot extrusion process, Mater. Charact. 92 (2014) 77–83.
[25] J. Bohlen, S.B. Yi, D. Letzig, K. Kainer, Effect of rare earth elements on the microstructure and texture development in magnesium-manganese alloys during extrusion, Mater. Sci. Eng. A 527 (2010) 7092–7098.
[26] T. Laser, C. Hartig, M.R. Nürnberg, D. Letzig, R. Bormann, The influence of calcium and cerium mischmetal on the microstructural evolution of Mg-3Al-1Zn during extrusion and resulting mechanical properties, Acta Mater 56 (2008) 2791–2798.
[27] K. Hantzsche, J. Bohlen, J. Wendt, K.U. Kainer, S.B. Yi, D. Letzig, Effect of rare earth additions on microstructure and texture development of magnesium alloy sheets, Scr. Mater 63 (2010) 725–730.
[28] M. Kaseem, B.K. Chung, H.W. Yang, K. Hamad, Y.G. Ko, Effect of deformation temperature on microstructure and mechanical properties of AZ31 Mg alloy processed by differential-speed rolling, J. Mater. Sci. Technol. 31 (2015) 498–503.